International Journal of Biological Macromolecules 186 (2021) 218–226

Contents lists available at ScienceDirect

International Journal of Biological Macromolecules

journal homepage: www.elsevier.com/locate/ijbiomac

Eco-friendly isolation and characterization of nanochitin from different origins by microwave irradiation: Optimization using response surface methodology

Rut Fernández-Marín [a], Fabio Hernández-Ramos [a], Asier M. Salaberria [a], Mª. Ángeles Andrés [a], Jalel Labidi [a,*], Susana C.M. Fernandes [b,*]

[a] Environmental and Chemical Engineering Department, University of the Basque Country UPV/EHU, Plaza Europa 1, 20018 Donostia-San Sebastián, Spain
[b] Universite de Pau et des Pays de l'Adour, IPREM, E2S UPPA, 64600 Anglet, France

ARTICLE INFO

Keywords:
Microwave irradiation
Alpha-chitin nanocrystals
Beta-chitin nanofibres

ABSTRACT

The extraction of nanochitin from marine waste has attracted great industrial interest due to its unique properties, namely biodegradability, biocompatibility and as a functional reinforcing agent. Conventional acid hydrolysis isolation of nanochitin requires high temperatures and acid concentration, time and energy. Herein, for the first time, microwave irradiation method was used as an eco-friendly approach to isolate nanochitin from different sources. The isolation conditions were optimized through an experimental Box-Behnken design using surface response methodology. The data showed optimal conditions of 1 M HCl, 10.00 min and 124.75 W to obtain lobster nanocrystals; 1 M HCl, 14.34 min and 50.21 W to obtain shrimp nanocrystals; and 1 M HCl, 29.08 min and 54.08 W to obtain squid pen nanofibres, reducing time and HCl concentration. The obtained isolation yields where of 85.30, 79.92 and 80.59 % for lobster, shrimp and squid, respectively. The morphology of the nanochitins was dependent of the chitin origin, and the lengths of the nanochitins were of 314.74, 386.12 and > 900 nm for lobster, shrimp and squid pen, respectively. The thermal stability of the ensuing nanochitins was maintained after treatment. The results showed that nanochitin could be obtained by using an eco-friendly approach like microwave irradiation.

1. Introduction

In recent years, the production of fishery by-products has considerably risen causing serious environmental problems due to its high chemical oxygen demand and presence of fats, pathogens, and others [1]. Nonetheless, because of the high content in proteins, minerals and polysaccharides present in these by-products, it has been observed an increasing interest in their valorisation [1,2]. Among the marine-derived polysaccharides, chitin (CH, poly β-(1–4)-*N*-acetyl-D-glucosamine), obtained mainly from seafood wastes like shrimp, crab, lobster and squid pen is renewable and abundant, and, in a near future, chitin will become one of the most important organic raw materials [3–5].

Being a supporting material in living organisms, chitin presents a highly-organized micro- and nanofibril structure, which contains crystalline and amorphous domains [4,6–8]. Depending on its origin and under controlled extraction conditions, it is possible to isolate chitin microfibrils in the form of nanocrystals (6–60 nm in width and 100–800 nm in length) and nanofibres (10–100 nm in width and many micrometres in length) in the alpha form (α), which is the most common, contains alternate antiparallel chains or beta form (β) that is formed by parallel chains [6,8,9]. Several studies have demonstrated the advantages of their unique properties such as small size, low density, high surface area, good chemical reactivity, biocompatibility, biodegradability, low toxicity, antimicrobial and antioxidant activity, and excellent mechanical performance [10,11]. These qualities generate a high interest in different industrial sectors (e.g. cosmetics, medical and food industries) as functional and reinforcing agents in nanotechnology and materials science [9,12].

For the isolation of nanochitin, from the extracted macroscopic chitin, the 'top-down' strategy is the most common and refers to the isolation of nanostructured crystals or fibrils via chemical or physical methods. For instance, the most popular of conventional methods to isolate chitin nanocrystals is strong acid hydrolysis. On the other hand, chitin nanofibres have been obtained by mechanical approach or by

* Corresponding authors.
E-mail addresses: jalel.labidi@ehu.es (J. Labidi), susana.fernandes@univ-pau.fr (S.C.M. Fernandes).

https://doi.org/10.1016/j.ijbiomac.2021.07.048
Received 14 January 2021; Received in revised form 5 July 2021; Accepted 6 July 2021
Available online 9 July 2021

ultrasonic technique [6,7,13]. Nonetheless, these treatments require high temperature and long reaction times, which implicates high-energy consumption [13–15]. There is an evident need of new eco-friendly and sustainable alternatives for the extraction of nanochitin.

An alternative methodology could be the microwave-assisted extraction (MAE) irradiation that presents low energy consumption, fast reaction and high production yield. The MAE consists of applying an electromagnetic field to a sample with polar solvents. The electromagnetic waves cause the dipoles of the molecules to try to align themselves with the field and produce frictions and collisions that raise the temperature [16,17]. Some researchers reported the extraction of chitin or chitosan with microwave irradiation technique. For instance, in a study realised by [18], the extraction time of α- and β-CH and chitosan decreased from 6–10 h to 10–15 min by using microwaves approach. Similarly, [3] achieved α-chitin and chitosan from shrimp, reducing the extraction time to 24 min by microwave. Also, [19] showed an experimental design where the demineralization step was optimized to obtain α-chitin from lobster employing 23 min under microwave irradiation. However, to the best of our knowledge, no literature was found related with the isolation of nanochitin by using microwave methodology.

In this context, in the present study, we propose to optimize the isolation conditions of α-chitin nanocrystals from shrimp and yellow lobster and β-chitin nanofibres from squid pen by using the microwaves irradiation methodology through an experimental Box-Behnken design using surface response methodology. The chemical structure, crystalinity, thermostability and morphology of the nanochitin were also assessed.

2. Materials and methods

2.1. Raw materials and chemicals

Powder α-chitin from shrimp shells (α-CH_S) and powder β-chitin from squid pens (β-CH_{SP}) were kindly supplied by Mahtani Chitosan PVT Ltd., India. Powder α-chitin from yellow lobster (*Cervimunida johni*) shells (α-CH_L) was extracted *in-house* based on our previous Works [20,21]. Antarctic Seafood S.A. (Chile) kindly provided the yellow lobster shell wastes. Hydrochloric acid (HCl, 37%, ACS reagent) was purchased from Sigma-Aldrich.

2.2. Experimental design of microwave-assisted isolation of nanochitin

2.2.1. General experimental procedure

Each chitin sample (1 g) was hydrolysed under vigorous stirring by microwave irradiation technique (Discover system, CEM, USA). The reaction conditions were adapted from the previously reported protocol [20] by using variable concentration of hydrochloric acid from 1 to 3 M (Tables 1 & 2) and a fixed chitin:HCl ratio (CH:HCl) of 1:30 *w/v*. After MAE, each reaction mixture was stopped by diluting it with ice-bath and washed twice by filtration. The reaction mixtures were finally dialyzed against distillate water (Regenerated Cellulose dialysis tubing: MWCO 12–14 kDa) until the pH of the surrounding bath remained stable (pH 5).

Table 1
List of the experimental variables involved in the microwave-assisted isolation of nanochitin.

Variable		Nomenclature	Units	Value or range
Fixed	CH:HCl	Ratio	g/mL	1:30
Independent	HCl concentration	HCl	M	1–3
	Reaction time	t	min	10–30
	Microwave power	P	W	50–200
Dependents	Nanochitin isolation yield	Y_L	%	–
		Y_S		
		Y_{Sq}		

The samples were then stored in refrigerator at 4 °C until analysed. Three different nanochitin samples - (i) α-nanochitin from lobster (α-NCH_L), (ii) α-nanochitin from shrimp (α-NCH_S), and (iii) β-nanochitin from squid pen (β-NCH_{SP}) - were obtained.

2.2.2. Experimental design and determination of the optimal isolation conditions

Response surface methodology (RSM) was used to analyse the effect of HCl concentration (HCl, M), reaction time (t, min) and microwave power (P, W) on the isolation yield of nanochitin: α-NCH_L, α-NCH_S and β-NCH_{SP}. A Box-Behnken Design (BBD), which consists of 15 experiments of which 3 corresponds to the replicates in the central point, was selected for the experimental design and optimization. The experimental design was created and the optimum conditions were predicted with the desirability function of Statgraphics Centurion version XV software (StatPoint Technologies INC., Warrento, VA, USA). Regression analysis function of Microsoft Excel Add-In, USA was employed to fit the experimental data obtained in the experimental design.

In order to adjust the experimental data a second-order polynomial equation was employed as described in Eq. (1):

$$y_j = \beta_0 + \sum_{i=1}^{k} \beta_i X_i + \sum_{i=1}^{k} \beta_{ii} X_i^2 + \sum \sum_{i<j=1}^{k} \beta_{ij} X_i X_j + \varepsilon \quad (1)$$

where K represents the number of factors (3), Y represents the dependent variables: Y_L (%, Yield of α-NCH_L), Y_s (%, Yield of α-NCH_S) and Y_{Sq} (%, Yield of β-NCH_{SP}). β_0, β_i, β_{ii} and β_{ij} represent the regression coefficient calculated from the experimental results employing the least-squares method, X_i and X_j are the dimensionless and normalized independent variables, which present variation ranges from −1 to 1 and ε is the experimental error. The model was validated by evaluating the lack of fit, the coefficient of determination (R^2), significance of the regression coefficients, the F-test value acquired from the analysis of variance (ANOVA).

The experimental variables implicated in the study are outlined in Table 1, which includes the fixed and independent variables and their values or range. The dependent variables that correspond to the nanochitin yields obtained from lobster (Y_L), shrimp (Y_S) and squid pen (Y_{Sq}) are also listed.

The isolation yields of nanochitins were determined according to the method of [22] with slight modifications (Eq. (S1), Supplementary material).

2.3. Characterization of the raw materials and isolated nanochitin

2.3.1. Attenuated total reflection-Fourier transform infrared radiation (ATR-FTIR)

The ATR-FTIR spectra of shrimp, lobster and squid pen powder chitin and of the obtained nanochitin were collected to analyse their chemical structure by using a Perkin Elmer Spectrum FT-IR spectrometer (Waltham, MA, USA). A total of 64 scans were accumulated in transmission mode with a resolution of 4 cm^{-1}. The spectra were recorded from a range of 600–4000 cm^{-1} using ATR mode of operation following the method of [23].

2.3.2. ^{13}C-Nuclear magnetic resonance spectroscopy (^{13}C NMR)

Solid-state ^{13}C nuclear magnetic resonance spectroscopy (^{13}C NMR) was recorded using a Bruker Advance III 400WBplus (MHZ) (Bruker, USA) spectrometer to obtain the lobster, shrimp and squid pen chitin and nanochitin at the optimal isolation conditions spectra following [25] method. The degree of *N*-acetylation (DA %) was estimated according to the [24] method (Eq. (S2), Supplementary material).

2.3.3. The X-ray diffraction (XRD)

The samples were analysed by XRD spectra using a Philip X'pert Pro automatic diffractometer (Phillips N.V., Amsterdam, Netherlands)

Table 2
Box-Behnken experimental design with operational conditions expressed in terms of dimensional and dimensionless independent variables HCl (HCl concentration, M) (X_1); t (time, min) (X_2); P (power, W) (X_3) and experimental responses obtained for dependent variables (nanochitin yield: Y_L, Y_S and Y_{Sq}).

Experiments	Independent variables			Normalized variables			Dependent variables		
	HCl (M)	t (min)	P (W)	X_1	X_2	X_3	Y_L	Y_S	Y_{Sq}
1	3	20	50	1	0	−1	83.71	75.03	68.57
2	2	20	125	0	0	0	85.47	71.03	73.30
3	1	20	50	−1	0	−1	88.42	77.85	76.60
4	2	10	50	0	−1	−1	87.73	78.61	71.91
5	1	30	125	−1	1	0	89.33	68.62	74.72
6	1	10	125	−1	−1	0	90.56	76.55	76.35
7	3	10	125	1	−1	0	88.25	49.71	70.98
8	2	30	50	0	1	−1	84.84	61.80	70.86
9	3	30	125	1	1	0	83.33	56.09	47.77
10	2	20	125	0	0	0	85.86	70.55	70.49
11	1	20	200	−1	0	1	89.20	76.53	74.10
12	2	10	200	0	−1	1	86.76	74.56	72.32
13	3	20	200	1	0	1	82.98	64.50	51.27
14	2	30	200	0	1	1	85.04	57.60	54.35
15	2	20	125	0	0	0	86.22	72.47	70.58

following the [25] method. The data was scanned in the 2θ angles from 5 to 70° using Cu-Kα radiation at 40 mA and 40 kV. The crystallinity index (C.I. %) was determinate according to the the [18] method (Eq. (S3), Supplementary material).

2.3.4. Thermogravimetric analysis (TGA)

The thermal properties of the native chitin and nanochitin samples were carried out in a TGA/SDT 851 Mettler Toledo instrument (Mettler Toledo, New Castle, USA) following [23]. For the analysis, 6 mg of each sample were used and were heated from room temperature to 800 °C at a constant rate of 10 °C min^{-1} under a nitrogen atmosphere with the flow rate of 20 mL min^{-1}.

2.3.5. Atomic force microscopy (AFM)

This technique was used to assess the morphology and size distribution of the obtained nanochitins. AFM pictures were collect using a Dimension 3100 NanoScope IV (Veeco, USA) following [25]. The images were scanned at room temperature using tapping mode with silicon nitride cantilever and 10 nm tip nominal radius at a frequency of 1 kHz. Ten measurements in random locations of each sample were done and the average length and width values were then calculated with NanoScope Analysis 1.9 software.

3. Results and discussion

3.1. Optimization of the isolation conditions for obtaining nanochitin

Conventional nanochitin isolation involves long and hard hydrolysis conditions, namely, the use of high concentration of HCl and time. These parameters affect the final nanochitin yields and properties, as well as the cost and environmental impact. Thus, it is crucial to find novel sustainable approaches to isolate nanochitin from chitin and optimize its isolation. Herein, the combination of response surface methodology and Box-Behnken design was used in order to optimize the isolation conditions, taking into account the most influential variables in the process (HCl concentration, reaction time and microwave power) to obtain the most interesting nanochitin yields of 3 different chitin origins, using an eco-friendly approach: microwave-assisted irradiation. Microwave irradiation was chosen because of lower energy consumption, shorter reaction times and higher yields. Table 1 lists the experimental plan including the fixed variable (CH:HCl ratio), the independent variable (concentration of HCl; t and P) and the dependent variables (nanochitin yields: Y_L, Y_S and Y_{Sq}). A summary of the set of experiments that were designated by the Statgraphics software, as well as the experimental results obtained for the dependent variables is shown in Table 2.

The determination coefficient R^2 indicates the validity of the design by explaining the total variations of the model [26,27]. Thus, as can be seen in Table S1 (Supplementary material), the determination coefficients R^2 obtained for nanochitin from lobster (α-NCH_L) and from squid pen (β-NCH_{Sp}) were 0.9802 and 0.9905 respectively, indicating that only 0.0198% and 0.0095% of the total variations remain unexplained with the selected model. These values indicate that the selected model is adequate to represent the relationships between the selected variables. In addition, Fisher's F-test evaluates the model's predictive goodness. The samples from α-NCH_L and β-NCH_{Sp} showed F-experimental (27.5041 and 58.0143, respectively) higher than the F-critical values for 9 degrees of freedom. This confirms that the model is statistically relevant. On the other hand, in the case of nanochitin from shrimp α-NCH_S, although R^2 and F values (0.8122 and 2.4024, respectively) were significantly lower, can be considered suitable to validate the model.

It was shown that the isolation yields are dependent of the source of chitin (Table 2). Therefore, the yield ranged from 82.98% (exp. 13) to 90.56% (exp. 6) for α-NCH_L, from 49.71% (exp. 7) to 78.61% (exp. 4) for α-NCH_S, and from 47.77% (exp. 9) to 76.6% (exp. 3) for β-NCH_{Sp}. Also, the regression coefficients summarized in Table S1 (Supplementary material) showed different behaviour depending on the feedstock. For instance, in the case of β-NCH_{Sp}, the independent variables that showed more influence in the isolation yield were the HCl concentration (X_1) and the time (X_2) as well as the interaction between both and their quadratic effect. The quadratic effect of power (X_3^2) also demonstrated influence with a 95% confidence interval. In the case of α-NCH_S, only two variables were significantly relevant (>90%), the linear effect of temperature and the quadratic effect of time An explanation for this could be the low adjustment showed by the design (R^2 = 82.64%). Finally, for α-NCH_S, all independent variables, as well as the interaction between them and their quadratic effects influenced the isolation yield.

3.2. Isolation yield

The interaction between the independent variables and their influence on the α-NCH_L, α-NCH_S and β-NCH_{Sp} isolation yields are shown in Fig. 1.

Fig. 1-1 displays the influence of the independent variables time (X_2) and power (X_3) on the samples yield when the HCl concentration was set to the midpoint value (X_1 = 0). This figure shows that time had a significant influence on the obtained nanochitin yield, the latter increase with the decrease of the reaction time. Nonetheless, due to the different contributions of the quadratic coefficients of time in the regression equation (see Table S1, Supplementary material), two different behaviours are differentiated between the samples: (1) in α-NCH_L sample (Fig. 1-1a) a slight decrease in yield is observed as the time reduces to a

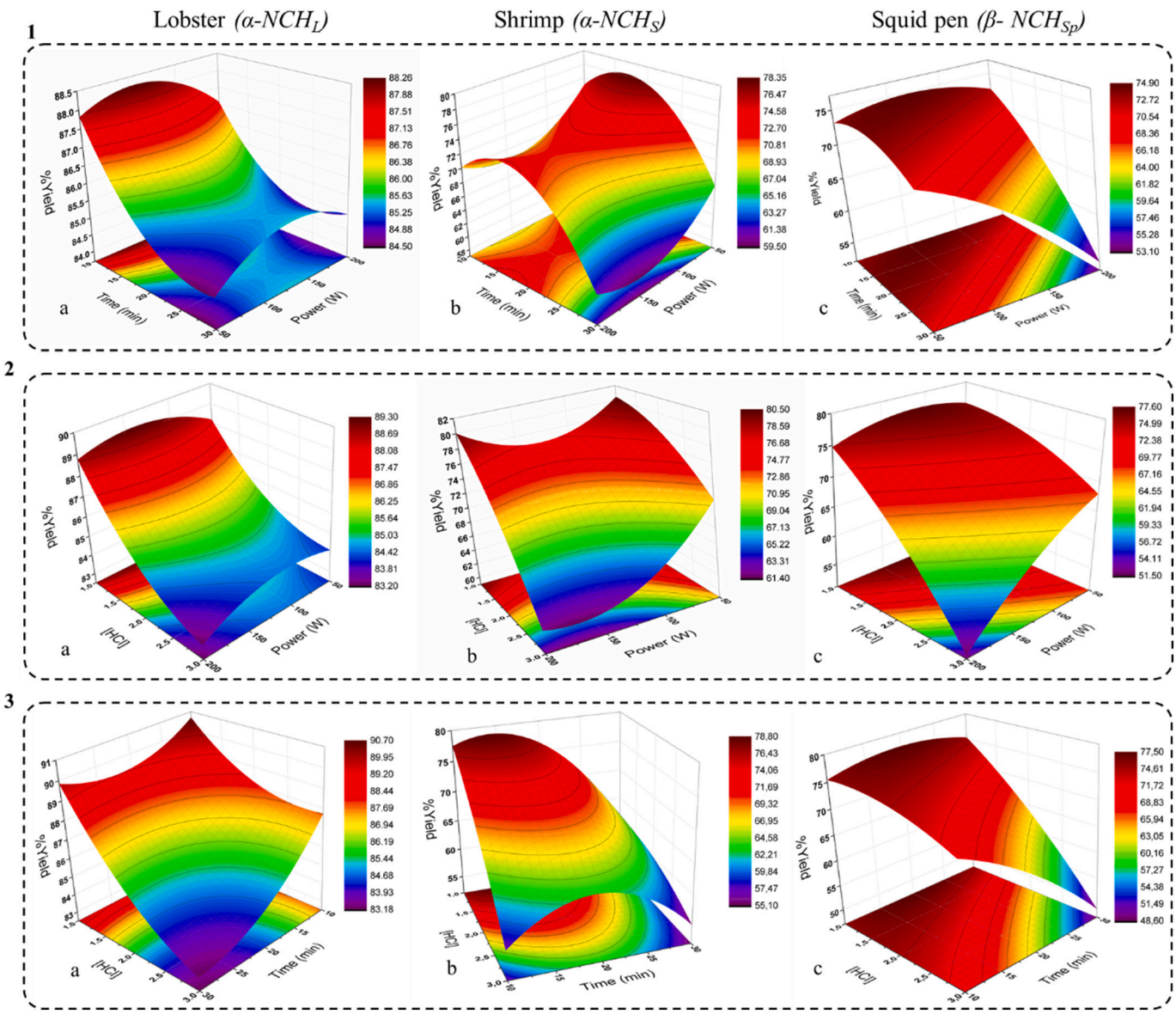

Fig. 1. Isolation yield as a function of: 1) time (t) and power (P) at a fixed HCl concentration (HCl) ($X_1 = 0$); 2) HCl concentration (HCl) and power (P) as a fixed time ($X_2 = 0$); 3) time (t) and HCl concentration (HCl) at a fixed power (P) (X_3) for: a) α-NCH$_L$, b) α-NCH$_S$ and c) β-NCH$_{Sp}$.

minimum, after which a decrease in reaction time leads to an increase in yield, this is explained by the positive contribution of the quadratic coefficient of time; and (2) in α-NCH$_S$ (Fig. 1-1b) and β-NCH$_{Sp}$ (Fig. 1-1c) samples, the opposite effect is observed due to the negative contribution of this coefficient meaning that the yield increased to a maximum as the reaction time decreased, after which a diminution in time decreased the yield. This behaviour was most pronounced for chitin shrimp feedstock (Fig. 1-1b). Interestingly, the data indicated that power (P, W) does not show a major influence on the isolation yield of α-NCH$_L$ and α-NCH$_S$ samples; however, for the β-NCH$_{Sp}$ sample the results indicated that an increase in power dramatically decrease the yield. Only in this case the independent variable power shows influence on the model (Table S1).

The independent variable X_3 exhibit the same behaviour in Fig. 1-2, in which the influence of the HCl concentration and power when the time value was fixed at a middle point value ($X_2 = 0$) is displayed. In this case, it should be noted that a reduction on the HCl concentration increased the obtained isolation yield in all samples. In addition, the lowest yield in all three cases was obtained when the HCl concentration and the microwave power were at their maximum levels. However, while in the case of α-NCH$_L$ (Fig. 1-2a) at high HCl concentration a drop in the power does not have a relevant influence in the obtained nanochitin yield, in the case of α-NCH$_S$ (Fig. 1-2b) and β-NCH$_{Sp}$ (Fig. 1-2c) the yield was increased substantially by decreasing the power.

Finally, the relationship between the independent variables that most influence the model, time and HCl concentration, by keeping the power at the midpoint ($X_3 = 0$) is represented in Fig. 1-3. This figure showed that a decrease in the HCl concentration together with low reaction times have a positive effect on obtaining nanoforms. Nonetheless, slight differences can be noticed among the three samples. On the one hand, in the case of α-NCH$_L$ (Fig. 1-3a) the yield decreases when the reaction time is reduced, but due to the positive contribution of the quadratic coefficient of time the trend changes and the yield increases, obtaining the maximum yield with minimum HCl concentration and reaction time. Nevertheless, for α-NCH$_S$ and β-NCH$_{Sp}$, Fig. 1-3b and -3c, respectively, in which the contribution of the quadratic coefficient of time is negative, the tendency is just the opposite. This means that the yield first rises as the time goes down to a maximum and afterwards it decreases.

3.3. Optimization of isolation conditions and validation of the model

The aim of the optimisation was to determine the optimal conditions for maximising the isolation yield of nanochitin from different chitin sources used in this study. Therefore, the dimensionless and dimensional values of the independent variables obtained through Statgraphics Centurion XV software are summarized in Table 3.

A triplicate of the experiments was performed to validate the model under optimal conditions. A comparison was made between the obtained results and the theoretical ones (Table 3). The experimental results are in agreement with those predicted by the software, which validates the selected design (Box-Behnken).

Authors such as Yuan et al., who studied the isolation of nanocrystals from crab shells, obtained similar yields. In this study, different isolation yields between 78 and 87.5 % were obtained by ultrasonic treatment among 1 and 3 h [28]. Other authors such as [29] showed lower isolation yields (55–60%) when acid hydrolysis with 3 M HCl at 100 °C was performed during 3 h for the isolation of crab nanocrystals. Other authors showed that the isolation yield of nanochitin is usually in the range of 40 to 86 % and for the CHNF is between 75 and 84 % depending on the reaction time and the source of chitin [30–32]. These results demonstrated that similar yields to traditional methods could be obtained by reducing the reaction time using the microwave technique.

3.4. Characterization of the ensuing Nanochitin

3.4.1. Chemical structure and crystallinity

The chemical structure of the samples was assessed by ATR-FTIR and by ^{13}C NMR (Fig. 2).

3.4.1.1. ATR-FTIR. As shown in Fig. 2-a, there were no changes in the ATR-FTIR spectra when the raw chitin samples and the isolated nanochitin samples were compared.

α-CH bands from lobster and shrimp and their corresponding α-NCH_L, α-NCH_S showed similar bands around at 3438 cm^{-1} and 3260 cm^{-1} corresponding to the O—H and N—H stretching vibrations. The amide II and amide III were observed around 1554 cm^{-1} and 1309 cm^{-1}, respectively [33,34].

Regarding the FTIR spectra of β-CH and β-NCH_{Sp}, they displayed similar absorption bands. For both, it was observed the band at 3278 cm^{-1} and 2875 cm^{-1} corresponding to the O—H and C—H stretching vibration; the peaks at around 1549 cm^{-1} corresponding to amide II; the bands at 1374 cm^{-1} and 1308 cm^{-1} assigned to the stretching band of C—H of methyl groups; and the peak at 1027 cm^{-1} corresponding to C—O stretching [35,36].

Interestingly, it was observed a difference between the α- and β-structures in the amide I band. In the α-chitin structure spectrum, two distincted bands were observed around 1654 cm^{-1} and 1621 cm^{-1} that have been assigned to the single H-bonded and double H-bonded, respectively; whereas for the β-structure a unique single band was observed at around 1631 cm^{-1} [33,35].

3.4.1.2. ^{13}C NMR. Fig. 2-b shows the ^{13}C NMR spectra of α-NCH_L and α-NCH_S, β-NCH_{Sp}. In all samples, the methyl group (CH_3) was observed around 23 ppm and carbonyl group (C=O) at 173 ppm. The signals between 58 and 100 ppm were attributed to the carbon atoms of D-glucopyranosyl ring, where the peaks located at 104, 82, 61 and 55 ppm were assigned to C1, C4, C6 and C2, respectively, for all samples. The chemical shifts of C5 and C3 of α-NCH_L and α-NCH_S appeared as a doublet at 75 and 73 ppm because of the different configurations; nonetheless, the peaks of C3 and C5 (C5/C3) of β-NCH_{Sp} sample merged into single resonance at 75 ppm, which is typical of beta-chitin structures [4,37]. Interestingly, in the present solid-state ^{13}C NMR spectra, there are no protein peaks (C–O: 180 ppm; C–N: 55 ppm).

The values determined by Eq. (S2), (Supplementary material) [24] showed that α-NCH_L and α-NCH_S have a DA equal to 90 and 91 %, respectively, and 88 % for β-NCH_{Sp}. These results are in accordance with previous works about nanochitin isolated from different sources [25,38–41].

3.4.1.3. XRD. The XRD patterns of α-CH and α-NCH from lobster and shrimp and β-CH and β-NCH_{Sp} were employed for study their crystal structure (Fig. 3-a).

All the XRD patterns of shrimp and lobster were very similar. The diffractograms exhibited the typical diffraction pattern of both α-NCH (lobster and shrimp) in which 5 crystalline reflection were observed between the ranges 5–40 in 2θ. α-NCH_L and α-NCH_S demonstrated two narrow and strong crystalline peaks at 9.5 and 19.5° in the 2θ angles indexed as (020) and (110) planes. A smaller crystalline peak corresponding to the amorphous domains was observed at around 13° (021). Its low value was due to the amorphous part of the chitin has been removed under acid hydrolysis when obtaining the nanocrystals [8]. The other two peaks that were observed were 20.9° (120) and 23.4° (101) with a similar result as the one reported by [20].

On the other hand, the β-CH and β-NCH_{Sp} diffraction patterns were similar and exhibited two peaks wider than in α-CH and α -CHNC samples. These peaks appeared around 9.30° and 19.30° which corresponding with (010) and (1-10) planes [36,41].

The crystallinity index (C.I. %) of each samples was calculated by [18] (Eq. (S3), Supplementary material) and is shown in Fig. 3-a. The higher C.I. % values of the chitin nanocrystals and nanofibres compared with their respective chitin is related to the amorphous part that was removed.

The C.I. % of α-NCH_L (93.5 %) and α-NCH_S (85.2 %) showed very similar results compared to the ones obtained by different studies such as Salaberria et al. (chitin nanocrystals from lobster 90 %) and Goodrich et al. (chitin nanocrystals from shrimp 84.0 %), which were carried out using acid hydrolysis treatment [20,42].

Regarding the C.I. % results for β-CH and β-NCH_{Sp} values of 84.1 % and 84.5 % were obtained, respectively. A similar behaviour was reported by [43] using mechanical approaches.

The difference between the peak's shapes in diffraction patterns and the C.I. % values demonstrates that the alpha structure is more crystalline polymorph since its antiparallel chains are more compacted [18].

3.4.2. Thermostability

The chitins and the nanochitins thermograms profiles

Table 3
Dimensionless and dimensional values of the optimal point of the system and predicted and experimental values at optimum conditions of the nanochitin isolation. The yields experimental values were average ± standard deviation from three replications ($n = 3$).

	Optimal point							
	Dimensionless			Dimensional			Yield %	
	X_1	X_2	X_3	HCl (M)	t (min)	P (W)	Predict value	Experimental value
α-NCH_L	−1	−1	−0.0034	1	10.00	124.75	90.69	85.30 ± 0.37
α-NCH_S	−1	−0.5660	−0.9972	1	14.34	50.21	82.72	79.92 ± 0.24
β-NCH_{Sp}	−1	0.9082	−0.9456	1	29.08	54.08	78.27	80.59 ± 0.11

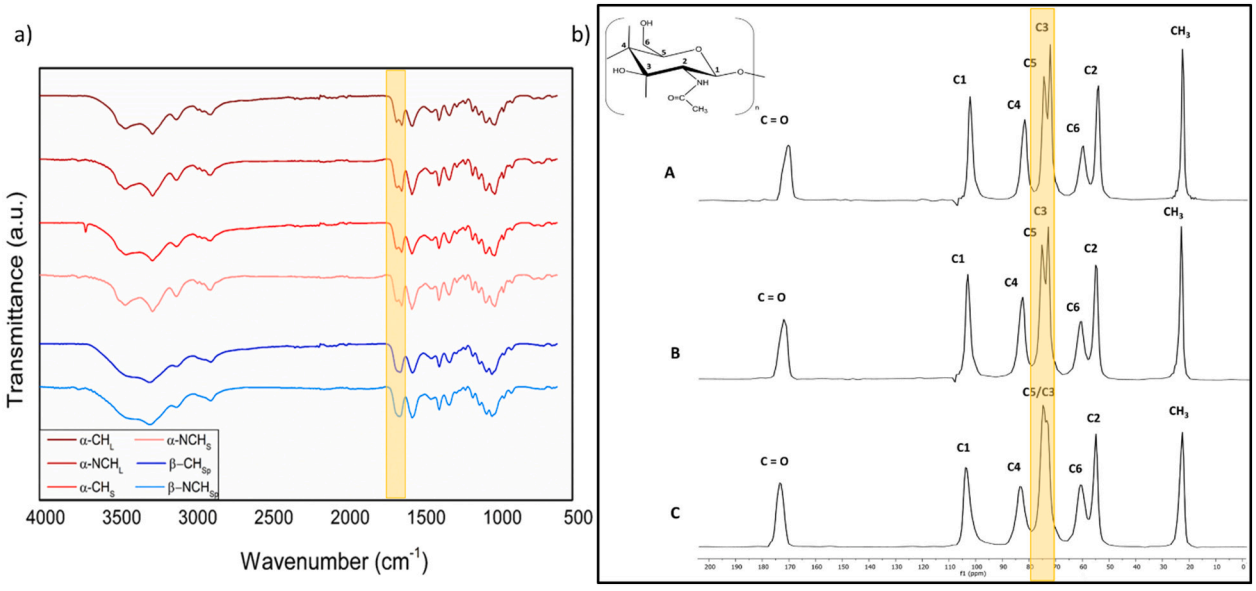

Fig. 2. a) ATR-FTIR spectra of the different samples and b) ^{13}C NMR spectra of: A) α-NCH_L, B) α-NCH_S and C) β-NCH_{Sp}.

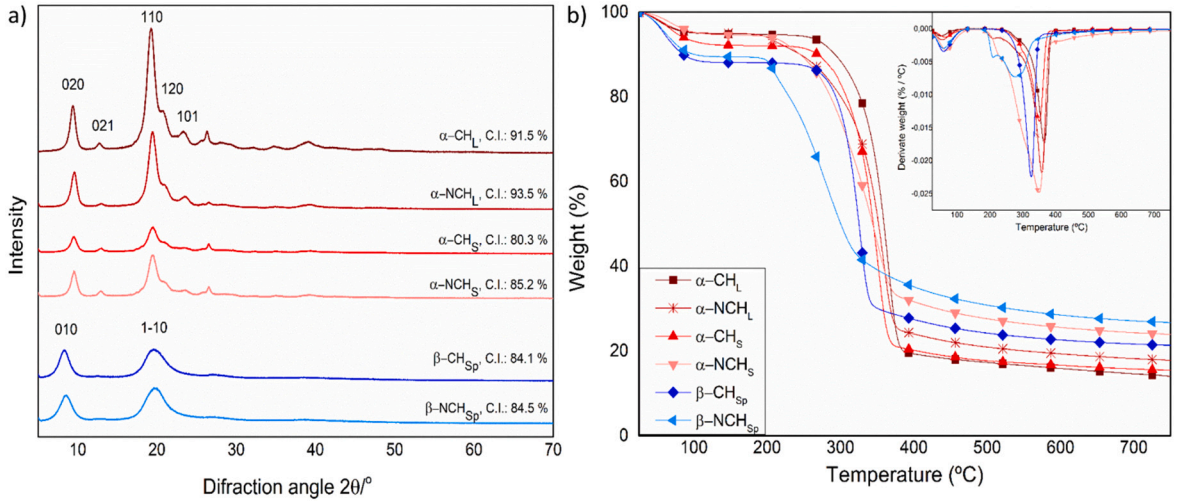

Fig. 3. a) XRD patterns and crystallinity index (C. I. %, [18]) and b) TGA and dTGA curves of α-CH_L, α-NCH_L, α-CH_S, α-NCH_S, β-CH_{Sp} and β-NCH_{Sp}.

(thermogravimetric analysis (TGA) and derivate (dTGA) are displayed in Fig. 3-b.

The first mass loss observed in both TGA and dTGA profiles of all samples at about 100 °C was assigned to the water evaporation and corresponds to a weight loss of 5–8 wt% for the α- chitin and around 10 wt% for the β-chitin [34]. The second mass loss, also observed in all samples, was attributed to the degradation of the chitin biopolymer corresponding to the degradation and dehydration of the polysaccharide structure and decomposition of the acetylated and deacetylated units of chitin polymer [34,38,44]. The dTGA profile (Fig. 3-b) showed the maximum degradation temperature around 350 °C and mass losses between 70 and 80 wt% for all samples with α-structure [38,45]. In contrast, lower maximum temperatures were observed for the samples of β-CH (329 °C) and β-NCH_{Sp} (281 °C) with mass losses of 60 and 70 wt %, respectively [46]. This difference between the two chitins polymorphs is due to the fact that β-structure contains slightly packed chains that require less heat for degradation [18,44].

Finally, TGA profiles demonstrated that the trend of nanocrystals and nanofibres samples were less thermostable than their respective native chitins. The same remark was done by [35], regarding the isolation of chitin nanocrystals from crab shells by the acid hydrolysis employing HCl during 3 h.

3.4.3. *Morphology of the obtained nanochitin*

The morphology and dimensions of nanochitin samples were analysed by AFM (Fig. 4). As expected, the α-NCH_L and α-NCH_S showed characteristic rod-like morphology. Interestingly, α-NCH_L exhibited shorter lengths and widths (average of 314.74 ± 62.50 nm in lengths and 41.62 ± 10.92 nm in width) than α-NCH_S (average of 386.12 ± 47.49 nm and 42.16 ± 4.62 nm in width). Similar results were reported by [32] that obtained shrimp nanocrystals with lengths of 200–560 nm and diameters of 18–40 nm and [20], that get lobster nanocrystals with lengths of 300 nm and diameters of 60 nm after acid hydrolysis. The aspect ratio (L/d) of α-NCH_L and α-NCH_S was of 7 and 9, respectively. Similar results were reported by [28] that obtained chitin nanocrystals with eutectic acid solvents (choline chloride and organic acids, such as citric, malonic, and lactic acid) with aspect ratios between 5 and 8.

On the other hand, the β-NCH_{Sp} samples exhibited long and fibrillar morphology with length superior to 900 nm and average diameter of 19.82 ± 1.16 nm. [47] demonstrated the same morphology and size for

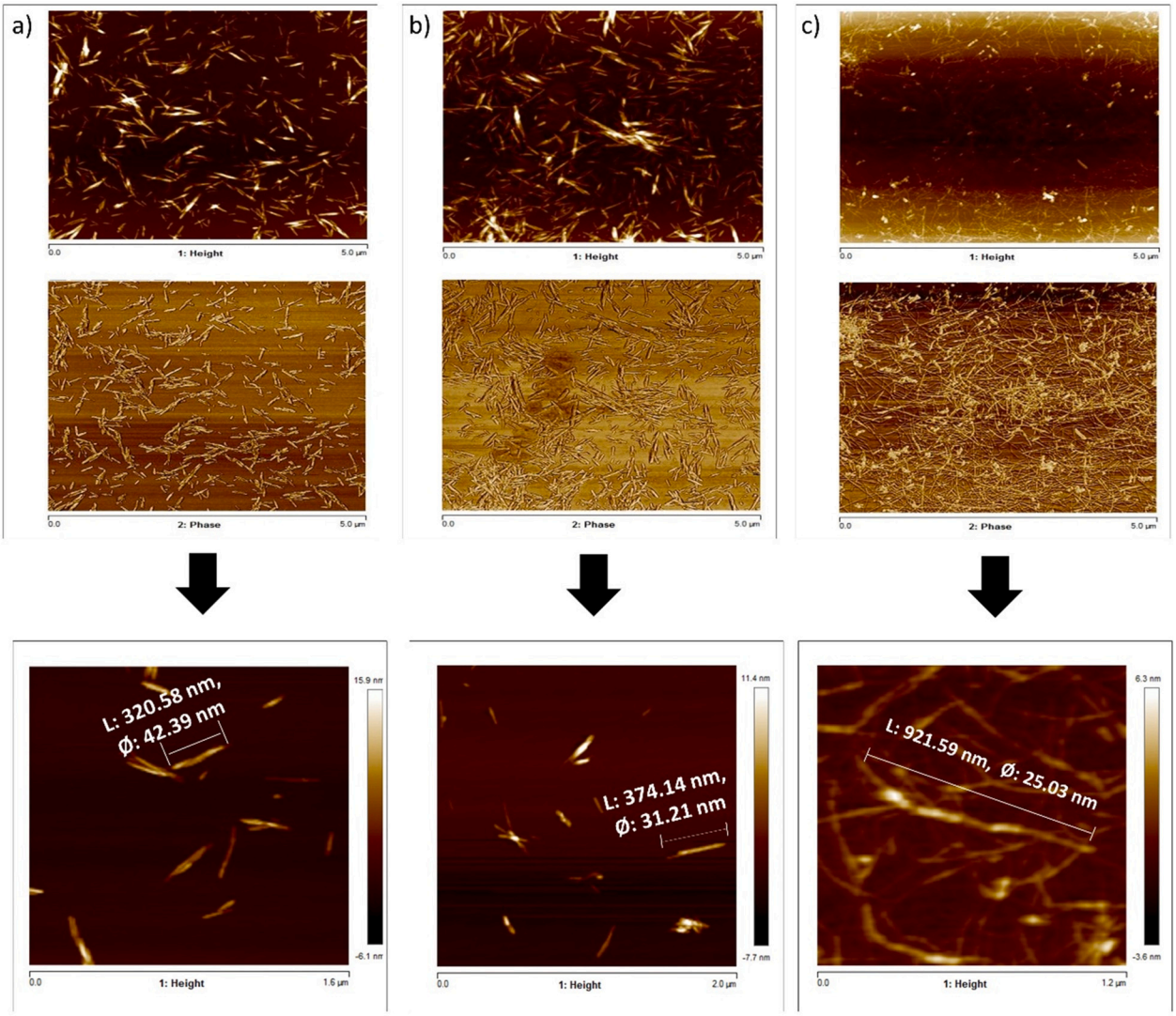

Fig. 4. Atomic Force Microscopy images in height (top) and phase (down) of a) α-NCH_L, b) α-NCH_S and c) β-NCH_{Sp}.

nanofibers isolated from squid pen using mechanical treatment. As expected, the aspect ratio for the β-NCH_{Sp} was much higher, with a value greater than 45.

4. Conclusions

The isolation of α-NCH_L, α-NCH_S and β-NCH_{Sp} was investigated for the first time and optimized by microwave-assisted extraction technique using the Box-Behnken design. The optimal isolation conditions were for α-NCH_L of 1 M HCl concentration, 10 min and 124.75 W; for α-NCH_S 1 M, 14.34 min and 50.21 W and for β-NCH_{Sp} 1 M, 29.08 min and 54.08 W. The predicted values of the optimal yield isolation values were in accordance with the experimental results, being 85.30, 79.92 and 80.59 % for α-NCH_L, α-NCH_S and β-NCH_{Sp}, respectively. The characterization of the samples demonstrated that chitin nanocrystals and nanofibers were successfully isolated. Moreover, the samples showed high C.I. % values and morphology similar to those obtained by conventional methods, such as acid hydrolysis, TEMPO-mediated oxidation or mechanical treatments. In addition, the reaction time was considerable reduced, with microwave-assisted extraction. Depending of the chitin source, the time can be reduced from 90 to 180 min using conventional chemical acid hydrolysis to 10–30 min and the HCl concentration can be decresed from 3 M to 1 M using microwave-assisted extraction.

Overall, the obtained data showed that nanocrystals and nanofibres could be obtained from different chitin sources by using an eco-friendly alternative like microwave irradiation technique. Such nanochitin samples could be used in different nanotechnologies and nanomaterials namely hydrogels, foams, porous scaffolds and polymeric nanocomposites.

CRediT authorship contribution statement

Conceptualization: J.L.; **Methodology** : R. F-M; A. M. S; **Formal analysis**: R. F-M; F. H-M; M. A. A. S; **Investigation**: R. F-M; **Resources**: M. A. A. S; J.L; **Data Curation**: R. F-M; A. M. S; S. S.C.M., F; **Writing - Original Draft**: R. F-M; F. H-M; **Writing - Review & Editing**: S. S.C.M., F; J.L.; **Visualization:** R. F-M; F. H-M; **Funding acquisition**: J.L.

Acknowledgments

The authors would like to thank the Basque Government (scholarship of young researchers training and project IT1008-16) for supporting financially this research and their gratitude for technical and human support provided by SGIker (UPV/EHU/ERDF, EU). S.C.M.F. is the recipient of an E2S UPPA Research Partnership Chair (MANTA: Marine Materials) supported by the "Investissements d'Avenir" French program managed by ANR (ANR-16-IDEX-0002), the Région Nouvelle-Aquitaine and the Communauté d'Agglomération du Pays Basque, France.

Appendix A. Supplementary data

The Supplementary data includes the calculation of the isolation yields, DA %, C.I. % and Table S1 with the regression coefficients and statistical parameters.

References

[1] H. El Knidri, R. Belaabed, A. Addaou, A. Laajeb, A. Lahsini, Extraction, chemical modification and characterization of chitin and chitosan, Int. J. Biol. Macromol. 120 (2018) 1181–1189, https://doi.org/10.1016/j.ijbiomac.2018.08.139.

[2] M. Claverie, C. McReynolds, A. Petitpas, M. Thomas, S.C.M. Fernandes, Marine-derived polymeric materials and biomimetics: an overview, Polymers 12 (2020), https://doi.org/10.3390/POLYM12051002.

[3] H. El Knidri, R. El Khalfaouy, A. Laajeb, A. Addaou, A. Lahsini, Eco-friendly extraction and characterization of chitin and chitosan from the shrimp shell waste via microwave irradiation, Process Saf. Environ. Prot. 104 (2016) 395–405, https://doi.org/10.1016/j.psep.2016.09.020.

[4] M. Rinaudo, Chitin and chitosan : properties and applications, Prog. Polym. Sci. 31 (2006) 603–632, https://doi.org/10.1016/j.progpolymsci.2006.06.001.

[5] B. Duan, Y. Huang, A. Lu, L. Zhang, Recent advances in chitin based materials constructed via physical methods, Prog. Polym. Sci. 82 (2018) 1–33, https://doi.org/10.1016/j.progpolymsci.2018.04.001.

[6] A.M. Salaberria, S.C.M. Fernandes, R.H. Diaz, J. Labidi, Processing of a-chitin nanofibers by dynamic high pressure homogenization: characterization and antifungal activity against a. niger, Carbohydr. Polym. 116 (2015) 286–291, https://doi.org/10.1016/j.carbpol.2014.04.047.

[7] A.M. Salaberria, J. Labidi, S.C.M. Fernandes, Different routes to turn chitin into stunning nano-objects, Eur. Polym. J. 68 (2015) 503–515, https://doi.org/10.1016/j.eurpolymj.2015.03.005.

[8] F. Larbi, A. García, J. Luis, A. Hamou, J. Puiggalí, Comparison of nanocrystals and nano fi bers produced from shrimp shell a - chitin : from energy production to material cytotoxicity and Pickering emulsion properties, Carbohydr. Polym. 196 (2018) 385–397, https://doi.org/10.1016/j.carbpol.2018.04.094.

[9] B. Joseph, R.M. Sam, P. Balakrishnan, H.J. Maria, S. Gopi, T. Volova, S.C. M. Fernandes, S. Thomas, Extraction of nanochitin from marine resources and fabrication of polymer nanocomposites: recent advances, Polymers 12 (2020), https://doi.org/10.3390/POLYM12081664.

[10] E. Jahed, M. Alizadeh, H. Almasi, R. Hasanzadeh, Physicochemical properties of Carum copticum essential oil loaded chitosan films containing organic nanoreinforcements, Carbohydr. Polym. 164 (2017) 325–338, https://doi.org/10.1016/j.carbpol.2017.02.022.

[11] H. Liu, W. Liu, B. Luo, W. Wen, M. Liu, X. Wang, C. Zhou, in: Electrospun Composite Nanofiber Membrane of Poly (l -Lactide) and Surface Grafted Chitin Whiskers : Fabrication, Mechanical Properties and Cytocompatibility 147, 2016, pp. 216–225.

[12] V. Zubillaga, A. Alonso-varona, S.C.M. Fernandes, A.M. Salaberria, T. Palomares, Adipose-derived mesenchymal stem cell chondrospheroids cultured in hypoxia and a 3D porous chitosan/chitin nanocrystal scaffold as a platform for cartilage tissue engineering, Int. J. Mol. Sci. 21 (2020) 1–17, https://doi.org/10.3390/ijms21031004.

[13] A.M. Salaberria, J. Labidi, S.C.M. Fernandes, Different routes to turn chitin into stunning nano-objects, Eur. Polym. J. 68 (2015) 503–515, https://doi.org/10.1016/j.eurpolymj.2015.03.005.

[14] C. Chen, D. Li, H. Yano, K. Abe, Bioinspired hydrogels: quinone crosslinking reaction for chitin nanofibers with enhanced mechanical strength via surface deacetylation, Carbohydr. Polym. 207 (2019) 411–417, https://doi.org/10.1016/j.carbpol.2018.12.007.

[15] Y. Ogawa, K. Azuma, H. Izawa, M. Morimoto, K. Ochi, T. Osaki, N. Ito, Y. Okamoto, H. Saimoto, S. Ifuku, Preparation and biocompatibility of a chitin nanofiber/gelatin composite film, Int. J. Biol. Macromol. 104 (2017) 1882–1889, https://doi.org/10.1016/j.ijbiomac.2017.02.041.

[16] R.D.Pinto Rodrigues, A.S.e Silva, T.A.V. Carlos, A.K.P. Bastos, R.S. de Santiago-Aguiar, M.V.P. Rocha, Application of protic ionic liquids in the microwave-assisted extraction of phycobiliproteins from Arthrospira platensis with antioxidant activity, Sep. Purif. Technol. 252 (2020), 117448, https://doi.org/10.1016/j.seppur.2020.117448.

[17] C.L. Teo, A. Idris, Evaluation of direct transesterification of microalgae using microwave irradiation, Bioresour. Technol. 174 (2014) 281–286, https://doi.org/10.1016/j.biortech.2014.10.035.

[18] F.A. Al Sagheer, M.A. Al-sughayer, S. Muslim, M.Z. Elsabee, Extraction and characterization of chitin and chitosan from marine sources in arabian gulf, Carbohydr. Polym. J. 77 (2009) 410–419, https://doi.org/10.1016/j.carbpol.2009.01.032.

[19] T.T. Nguyen, A.R. Barber, P. Smith, X. Luo, W. Zhang, Application and optimization of the highly efficient and environmentally-friendly microwave-intensified lactic acid demineralization of deproteinized rock lobster shells (Jasus edwardsii) for chitin production, Food Bioprod. Process. 102 (2017) 367–374, https://doi.org/10.1016/j.fbp.2017.02.005.

[20] A.M. Salaberria, J. Labidi, S.C.M. Fernandes, Chitin nanocrystals and nanofibers as nano-sized fillers into thermoplastic starch-based biocomposites processed by melt-mixing, Chem. Eng. J. 256 (2014) 356–364, https://doi.org/10.1016/j.cej.2014.07.009.

[21] A.M. Salaberria, R.H. Diaz, J. Labidi, S.C.M. Fernandes, Preparing valuable renewable nanocomposite films based exclusively on oceanic biomass – chitin nanofillers and chitosan, React. Funct. Polym. 89 (2015) 31–39.

[22] Y. Xiao, Y. Liu, X. Wang, M. Li, H. Lei, H. Xu, Cellulose nanocrystals prepared from wheat bran: characterization and cytotoxicity assessment, Int. J. Biol. Macromol. 140 (2019) 225–233, https://doi.org/10.1016/j.ijbiomac.2019.08.160.

[23] R. Fernández-Marín, J. Labidi, M.Á. Andrés, S.C.M. Fernandes, Using α-chitin nanocrystals to improve the final properties of poly (vinyl alcohol) films with Origanum vulgare essential oil, Polym. Degrad. Stab. (2020), 109227, https://doi.org/10.1016/j.polymdegradstab. 2020.109227.

[24] M.R. Kasaai, Determination of the degree of N -acetylation for chitin and chitosan by various NMR spectroscopy techniques: a review, Carbohydr. Polym. 79 (2010) 801–810, https://doi.org/10.1016/j.carbpol.2009.10.051.

[25] A.M. Salaberria, R.H. Diaz, J. Labidi, S.C.M. Fernandes, Role of chitin nanocrystals and nanofibers on physical, mechanical and functional properties in thermoplastic starch films, Food Hydrocoll. 46 (2015) 93–102, https://doi.org/10.1016/j.foodhyd.2014.12.016.

[26] B. Gullón, P. Gullón, T.A. Lú-chau, M. Teresa, J.M. Lema, Optimization of solvent extraction of antioxidants from Eucalyptus globulus leaves by response surface methodology: characterization and assessment of their bioactive properties, Ind. Crop. Prod. 108 (2017) 649–659, https://doi.org/10.1016/j.indcrop.2017.07.014.

[27] A. Morales, B. Gullón, I. Dávila, G. Eibes, J. Labidi, P. Gullón, Optimization of alkaline pretreatment for the co-production of biopolymer lignin and bioethanol from chestnut shells following a biorefinery approach, Ind. Crop. Prod. 124 (2018) 582–592, https://doi.org/10.1016/j.indcrop.2018.08.032.

[28] Y. Yuan, S. Hong, H. Lian, K. Zhang, H. Liimatainen, Comparison of acidic deep eutectic solvents in production of chitin nanocrystals, Carbohydr. Polym. 236 (2020), 116095, https://doi.org/10.1016/j.carbpol.2020.116095.

[29] J. Araki, Y. Yamanaka, K. Ohkawa, Chitin-chitosan nanocomposite gels: reinforcement of chitosan hydrogels with rod-like chitin nanowhiskers, Polym. J. 44 (2012) 713–717, https://doi.org/10.1038/pj.2012.11.

[30] B. Ma, A. Qin, X. Li, X. Zhao, C. He, Structure and properties of chitin whisker reinforced chitosan membranes, Int. J. Biol. Macromol. 64 (2014) 341–346, https://doi.org/10.1016/j.ijbiomac.2013.12.015.

[31] N.E. Mushi, N. Butchosa, M. Salajkova, Q. Zhou, L.A. Berglund, Nanostructured membranes based on native chitin nanofibers prepared by mild process, Carbohydr. Polym. 112 (2014) 255–263, https://doi.org/10.1016/j.carbpol.2014.05.038.

[32] S. Phongying, S. Chirachanchai, S. Ichi Aiba, Direct chitosan nanoscaffold formation via chitin whiskers, Polymer 48 (2007) 393–400, https://doi.org/10.1016/j.polymer.2006.10.049.

[33] N. Lin, S. Zhao, L. Gan, P.R. Chang, T. Xia, J. Huang, in: Preparation of Fungus-derived Chitin Nanocrystals and Their Dispersion Stability Evaluation in Aqueous Media 173, Carbohydr. Polym., 2017, pp. 610–618.

[34] S. Cao, W. Gu, W. Ou-yang, D. Chen, B. Yang, Y. Ma, Y. An, in: Preparation, Characterization and Application of Rod-like Chitin Nanocrystal by Using p-Toluenesulfonic Acid/Choline Chloride Deep Eutectic Solvent as a Hydrolytic Media 213, Carbohydr. Polym., 2019, pp. 304–310.

[35] S. Shankar, J.P. Reddy, J.W. Rhim, H.Y. Kim, Preparation, characterization, and antimicrobial activity of chitin nanofibrils reinforced carrageenan nanocomposite films, Carbohydr. Polym. 117 (2015) 468–475, https://doi.org/10.1016/j.carbpol.2014.10.010.

[36] H.N. Cuong, N.C. Minh, N. Van Hoa, T.S. Trung, Preparation and characterization of high purity ß-chitin from squid pens (Loligo chenisis), Int. J. Biol. Macromol. 93 (2016) 442–447, https://doi.org/10.1016/j.ijbiomac.2016.08.085.

[37] A. Oberemko, A.M. Salaberria, R. Saule, G. Saulis, M. Kaya, Physicochemical and in vitro cytotoxic properties of chitosan from mushroom species (Boletus bovinus and Laccaria laccata), Carbohydr. Polym. 221 (2019) 1–9, https://doi.org/10.1016/j.carbpol.2019.05.073.

[38] M. Kaya, I. Sargin, K.Ö. Tozak, T. Baran, S. Erdogan, G. Sezen, Chitin extraction and characterization from Daphnia magna resting eggs, Int. J. Biol. Macromol. 61 (2013) 459–464, https://doi.org/10.1016/j.ijbiomac.2013.08.016.

[39] J. Machida, S. Suenaga, M. Osada, Effect of the degree of acetylation on the physicochemical properties of a-chitin nanofibers, Int. J. Biol. Macromol. 155 (2020) 350–357, https://doi.org/10.1016/j.ijbiomac.2020.03.213.

[40] A. Tolaimate, J. Desbrières, M. Rhazi, A. Alagui, M. Vincendon, P. Vottero, On the influence of deacetylation process on the physicochemical characteristics of chitosan from squid chitin, Polymer 41 (2000) 2463–2469, https://doi.org/10.1016/S0032-3861(99)00400-0.

[41] O.I. Bogdanova, A.P. Istomina, N.A. Glushkova, S.I. Belousov, N.M. Kuznetsov, D. K. Polyakov, Effect of exfoliating agent on rheological behavior of ß -chitin fibrils in aqueous suspensions and on mechanical properties of poly (acrylic acid)/ ß -chitin composites, Int. J. Biol. Macromol. 139 (2019) 161–169, https://doi.org/10.1016/j.ijbiomac.2019.07.194.

[42] J.D. Goodrich, W.T. Winter, Alpha-Chitin nanocrystals prepared from shrimp shells and their specific surface area measurement, Biomacromolecules 8 (2007) 252–257.

[43] Q. Wu, E. Jungstedt, M. Šoltésová, N.E. Mushi, L.A. Berglund, High strength nanostructured films based on well-preserved ß-chitin nanofibrils, Nanoscale 11 (2019) 11001–11011, https://doi.org/10.1039/c9nr02870f.

[44] J.N.I. Balitaan, J.M. Yeh, K.S. Santiago, Marine waste to a functional biomaterial: green facile synthesis of modified-ß-chitin from Uroteuthis duvauceli pens (gladius), Int. J. Biol. Macromol. (2019), https://doi.org/10.1016/j.ijbiomac.2019.11.041.

[45] B.A. Juárez-De La Rosa, P. Quintana, P.L. Ardisson, J.M. Yáñez-Limón, J. J. Alvarado-Gil, Effects of thermal treatments on the structure of two black coral

species chitinous exoskeleton, J. Mater. Sci. 47 (2012) 990–998, https://doi.org/10.1007/s10853-011-5878-9.
[46] V. Aylanc, S. Ertosun, L. Akyuz, B. Koc Bilican, S. Gokdag, I. Bilican, Y.S. Cakmak, B.A. Yilmaz, M. Kaya, Natural ß-chitin-protein complex film obtained from waste razor shells for transdermal capsaicin carrier, Int. J. Biol. Macromol. 155 (2020) 508–515, https://doi.org/10.1016/j.ijbiomac.2020.03.232.
[47] I.F. Nata, T.M. Wu, J.K. Chen, C.K. Lee, A chitin nanofibril reinforced multifunctional monolith poly(vinyl alcohol) cryogel, J. Mater. Chem. B 2 (2014) 4108–4113, https://doi.org/10.1039/c4tb00175c.